

## Investigation on physical properties of $\text{Ni}_{0.6}\text{Zn}_{0.4}\text{Fe}_2\text{O}_4$ ferrite nanoparticles

P. S. Kumar<sup>a\*</sup>, G. K. Sivasankara Yadav<sup>b</sup>, V. K. Vamsi Krishna<sup>a</sup>,  
A. Thirupathi<sup>a</sup>, P. Yamuna<sup>a</sup>

<sup>a</sup> Department of Physics, Malla Reddy Engineering College (Autonomous),  
Secunderabad, T.S. - 500100, India

<sup>b</sup> Department of physics, Rayalaseema University, Kurnool, A.P, India

The nano  $\text{Ni}_{0.6}\text{Zn}_{0.4}\text{Fe}_2\text{O}_4$  ferrite nanoparticles have been synthesized by using sol-gel auto combustion method using citric acid as fuel agent calcined at different temperatures (400<sup>o</sup>C, 500<sup>o</sup>C and 600<sup>o</sup>C). The structural, dielectric and magnetic properties were examined by using X-ray diffraction (XRD), Field emission scanning electron microscope (FESEM), FTIR spectra, LCR meter and vibrating sample magnetometer (VSM). The single-phase cubic spinel structure of all samples confirmed from X-ray diffraction analysis. Surface morphology studies reveal that the grains are clear with well-defined grain boundaries and also found that the average grain size is maximum at 600<sup>o</sup>C calcination temperature. FTIR spectra confirm the phase of material at frequency bands (557 to 577  $\text{cm}^{-1}$ ). The highest saturation magnetization was found at a calcination temperature 600<sup>o</sup>C with value 80.39 emu/g, and the value coercive field ( $H_c$ ) was inverse with the crystallite size.

(Received January 31, 2021; Accepted April 4, 2021)

*Keywords:* Sol-gel auto combustion, LCR, VSM and Dielectric constant

### 1. Introduction

The spinel ferrites have concerned much attention in recent years due to their exceptional magnetic, electrical properties and chemical stabilities [1–3]. Nanoscale  $\text{NiFe}_2\text{O}_4$  is one of the versatile and technologically important soft ferrite materials with significant qualities such as low coercivity, high electrical resistivity and chemical stabilities, catalytic behaviour, etc. Because of these properties,  $\text{NiFe}_2\text{O}_4$  nanoparticles have various potential applications in magnetic fluids, electrodes, catalysis, sorbent, gas sensor, and biomedicine [4–8]. In general, the spinel ferrites attained a chemical formula is  $\text{AB}_2\text{O}_4$ , where ‘A’ and ‘B’ can indicate the tetrahedral and octahedral sites, respectively. In other words, the divalent cations such as  $\text{Ni}^{+2}$ ,  $\text{Mg}^{+2}$ ,  $\text{Zn}^{+2}$ ,  $\text{Co}^{+2}$ ,  $\text{Cu}^{+2}$  and  $\text{Mn}^{+2}$  can occupy the A-site while the B site can be occupied by trivalent cation like  $\text{Fe}^{+3}$  [9,10]. For example,  $\text{NiFe}_2\text{O}_4$  and  $\text{ZnFe}_2\text{O}_4$  can exhibit a cubic spinel structure [11,12]. Nevertheless, these spinel structures will be again classified into three types (normal spinel, inverse spinel and mixed spinel) based on the degree of inversion ( $0 < \delta < 1$ ). The  $\delta = 1$ ,  $\delta = 0$  and  $\delta = 0.25$  for normal spinel, inverse spinel and mixed spinels, respectively [13]. Normally, the degree of inversion was inter-linked to the cation distribution between A and B-sites. This cation distribution was observed to be different for bulk and nano ferrites. Both Ni and Zn ferrites are known to have a dominant preference for tetrahedral and octahedral locations, whereas nickel ferrite is an inverse spinel ferrite and zinc ferrite is a normal spinel ferrite. The composite Ni – Zn ferrites, however, are known to exist as a completely mixed spinel structure. The variation of elemental composition in these ferrites results in the redistribution of metal ions over the tetrahedral and octahedral sites, which can alter the properties of ferrites. The properties of these ferrite nanoparticles can also be tailored by altering parameters such as doping concentration or the synthesis process [14]. Because of this prepared NiZn ferrites are studied for distinct physical properties.

---

\* Corresponding author: sivakumar.pendyala@gmail.com

## 2. Experimental

The chemical formula of considered Mg-doped Zn ferrite is  $\text{Ni}_{0.6}\text{Zn}_{0.4}\text{Fe}_2\text{O}_4$  was prepared using the sol-gel auto combustion method. All used precursors are nitrates provided by Merck and Sigma Aldrich chemicals with AR grade having 99.5% purity. Magnesium nitrate  $[\text{Ni}(\text{NO}_3)_2 \cdot 6\text{H}_2\text{O}]$ , zinc nitrate  $[\text{Zn}(\text{NO}_3)_2 \cdot 6\text{H}_2\text{O}]$ , ferrous nitrate  $[\text{Fe}(\text{NO}_3)_3 \cdot 9\text{H}_2\text{O}]$  are precursors and citric acid  $[\text{C}_6\text{H}_8\text{O}_7 \cdot \text{H}_2\text{O}]$  act as burning agent and ammonia solution ( $\text{NH}_3$ ) is for maintaining the pH level of solution. The nitrates were dissolved using distilled water separately in a glass beaker. They were mixed into a large beaker using magnetic stirrer after the individual chemicals had been fully dissolved. After some time a clear solution was formed, maintain citric acid to nitrate ratio as 1:3 by adding two solutions. From the previous works of literature, we consider 1:3 molar ratio is suitable for obtaining less agglomeration and tiny sized particles. Maintaining pH value equal to 7 by adding ammonia ( $\text{NH}_3$ ) drop by drop under constant stirring. The previous works of literature also indicate that the size of the particles depends on the pH value. After a few hours, during the stirring and heating stage observed the homogenous solution. By continuous heating and stirring at  $150^\circ\text{C}$ , water molecules evaporated continuously after some time a dense and extremely sticky gel was found.

This gel was heated in the temperature range  $180^\circ\text{C}$ - $220^\circ\text{C}$ . After some time, evaporate the water molecules completely, at the time of instant observe the burning of gel automatically give rise to auto combustion, it is very quick due to the evolution of gaseous products. Moreover, after a while, the full gel transformed to ashes or smouldered, "erupting like a volcano from the lower of the beaker to the upper. This process was completed in no moment. The obtained powders colures in dark brown ash were produced at temperature  $250^\circ\text{C}$  in the form of a tree structure. Finally, the powder was cooled to room temperature. The complete preparation steps are shown in Fig.1 The agate mortar is used to grind the powder for 30 minutes, then samples are obtained in the form of incredible dense.

Finally obtained powder specimen is calcinated under standard circumstances at temperature  $400^\circ\text{C}$ ,  $500^\circ\text{C}$  and  $600^\circ\text{C}$  about 4 hours and maintain room temperature. Also, all prepared powder samples are tested for structural analyses, using XRD, SEM, FTIR and EDS techniques. Similarly, the electrical and magnetic properties studied with LCR and VSM instruments.

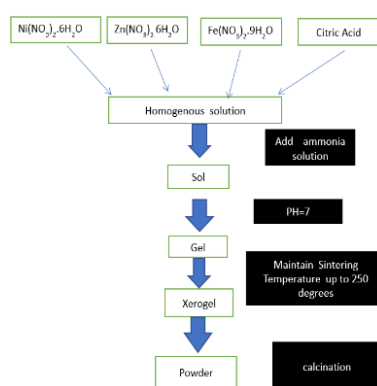


Fig. 1. Flow chart synthesis process of Ni-doped Zn Nanoparticles.

## 3. Results and discussion

### 3.1. Structural analysis

Fig. 2 illustrate XRD pattern of synthesized  $\text{Ni}_{0.6}\text{Zn}_{0.4}\text{Fe}_2\text{O}_4$  nano ferrite calcinated at  $400^\circ\text{C}$ ,  $500^\circ\text{C}$  and  $600^\circ\text{C}$  respectively. The XRD pattern of  $\text{Ni}_{0.6}\text{Zn}_{0.4}\text{Fe}_2\text{O}_4$  ferrite shows eight peaks situated in a range of  $20^\circ$  to  $80^\circ$  angle. The peak intensity equivalent to a structure is displayed in terms of % of miller indices as shown in Fig. 2. The obtained X-ray diffraction

pattern suitable with JCPDS card no.10-325. There was a change in the Zn ferrite structure with the addition of Ni content [15].

The pattern of  $\text{Ni}_{0.6}\text{Zn}_{0.4}\text{Fe}_2\text{O}_4$  can be indexed as a pure cubic spinel structure and found to the presence of secondary phases. The doping of Ni content, extra peaks arises corresponding to the nickel composition as indicating with the "♦" symbol shown in figure(2) [15]. The most intense (311) peak of cubic spinel ferrite observed as a measure of its degree of good crystallinity. The crystallite size (D) of  $\text{Ni}_{0.6}\text{Zn}_{0.4}\text{Fe}_2\text{O}_4$  sample was calculated by using the Scherrer formula is given by

$$D = \frac{K\lambda}{\beta \cos\theta} \quad (1)$$

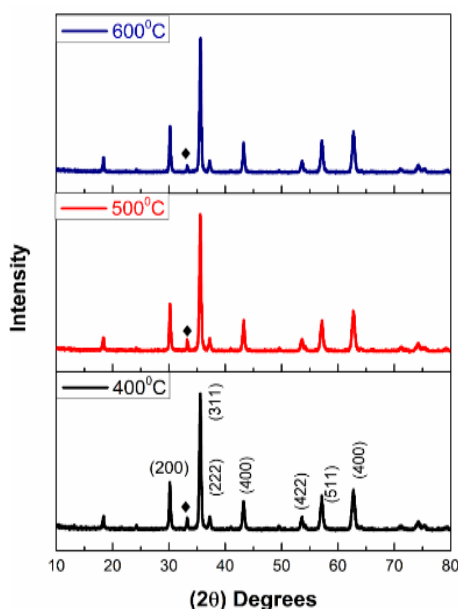


Fig. 2. XRD pattern of  $\text{Ni}_{0.6}\text{Zn}_{0.4}\text{Fe}_2\text{O}_4$  nanoparticles calcined at  $400^\circ\text{C}$ ,  $500^\circ\text{C}$  and  $600^\circ\text{C}$ .

where  $k=0.9$  is Scherrer's constant,  $\lambda = 1.5406 \text{ \AA}$  is the wavelength of the incident x-rays,  $\beta$  is the full width at half maximum (FWHM) of diffraction peak, and  $\theta$  is the Bragg's angle of diffraction.

Fig. 3 shows the variation of crystallite size with an increase of calcination temperature. The crystallite size (D) varies from 27.07 to 29.42 nm. The observed variation in the crystallite size is mainly due to that agglomeration of nanoparticles[16]. Unlike crystallite size, the lattice parameter values decrease with the increase of calcination temperature. The decreasing nature of lattice parameter values is due to the less ionic radii of  $\text{Ni}^{2+}$  ( $0.69\text{ \AA}$ ) ions substituted in place of large ionic radii of  $\text{Zn}^{2+}$  ( $0.74\text{ \AA}$ ) at tetrahedral sites at all calcination temperatures, as shown in Fig. 3. A similar type of behaviour was observed by Ashok Kumar in nickel Zinc ferrites [17].

The lattice parameter (a) of  $\text{Ni}_{0.6}\text{Zn}_{0.4}\text{Fe}_2\text{O}_4$  nanoparticles is determined by using equation

$$a = d\sqrt{h^2 + k^2 + l^2} \quad (2)$$

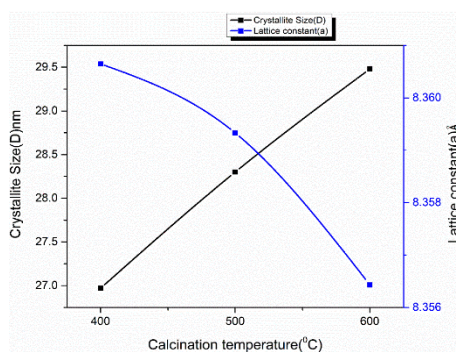


Fig. 3. Variation of crystallite size and lattice constant of  $Ni_{0.6}Zn_{0.4}Fe_2O_4$  ferrite nanoparticles at  $400^{\circ}C$ ,  $500^{\circ}C$  and  $600^{\circ}C$  calcination temperatures.

Table 1. Dependence of crystallite size ( $D$ ), lattice constant ( $a$ ) and unit cell volume ( $a^3$ ) of  $Ni_{0.6}Zn_{0.4}Fe_2O_4$  nanoparticles.

Composition (X)	Calcination temperature ( $^{\circ}C$ )	Crystallite size $D$ (nm)	Lattice constant $a$ (Å)	Volume of the Unit cell $a^3$ (Cm $^3$ )
$Ni_{0.6}Zn_{0.4}Fe_2O_4$	400	26.97	8.36065	584.41
	500	28.3	8.35933	584.13
	600	29.48	8.35643	583.52

### 3.2. SEM analysis

The SEM analysis is used to study the morphology of all the samples. Fig. 4 shows SEM micrographs of  $Ni_{0.6}Zn_{0.4}Fe_2O_4$  specimen. All micrographs showed the same magnifications. From the SEM images, it can be found that synthesized samples contain nanoparticles. Hence, the prepared nanoparticles look like spherical, dispersed and less agglomeration. From SEM study, the observations on grain size reveal that increasing nature with an increase of calcination temperature and changed like the XRD analysis.

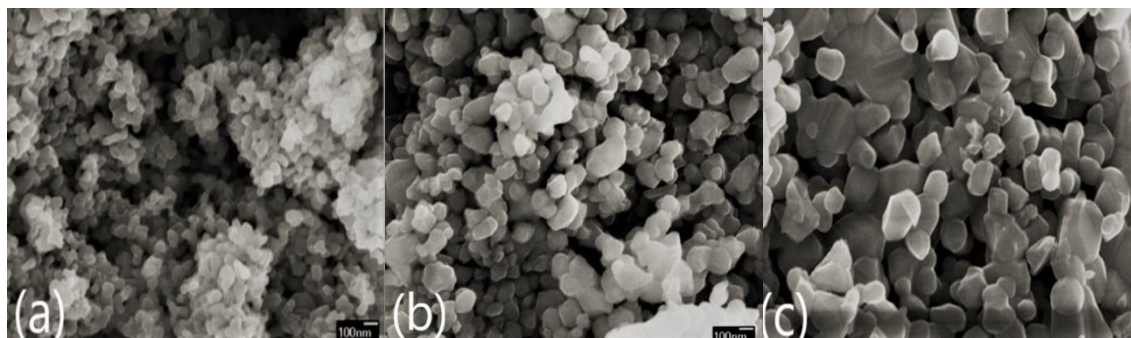


Fig. 4. (a, b & c) SEM micrographs of  $Ni_{0.6}Zn_{0.4}Fe_2O_4$  ferrite nanoparticles at  $400^{\circ}C$ ,  $500^{\circ}C$  and  $600^{\circ}C$  calcination temperatures.

### 3.3. EDS analysis

Fig. 5 shows the EDS spectrum for  $Ni_{0.6}Zn_{0.4}Fe_2O_4$  nano ferrite samples. EDS is one of the powerful tools for describing the percentage of elemental composition in the sample. Table 2 shows the list of elemental and atomic percentages of samples. All images indicate the presence of elements used for synthesizing such as atoms of Ni, Zn, Fe, and oxygen. No other impurity components present in the samples except for these elements, so that prepared samples are defect-free and homogenous.

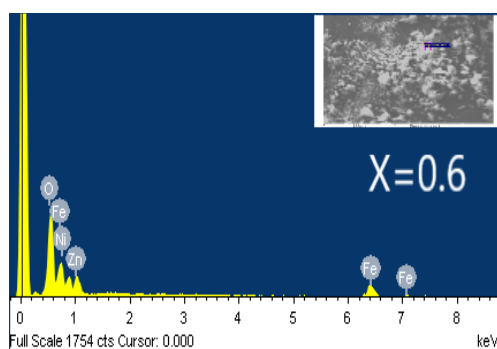


Fig. 5. EDS image for  $Ni_{0.6}Zn_{0.4}Fe_2O_4$  nano ferrite particles.

Table 2. Elemental and atomic percentages of  $Ni_{0.6}Zn_{0.4}Fe_2O_4$ .

Element (x)	O		Ni		Zn		Fe	
	Element %	Atomic %	Element %	Atomic %	Element %	Atomic %	Element %	Atomic %
0.6	26.24	56.25	13.26	6.62	11.62	6.1	45	27.64

### 3.4 FTIR analysis

Fig. 6 illustrates IR spectra for  $Ni_{0.6}Zn_{0.4}Fe_2O_4$  nano ferrite specimens calcined at  $400^{\circ}C$ ,  $500^{\circ}C$  and  $600^{\circ}C$  in the range between  $400$  to  $900\text{ cm}^{-1}$  at  $300K$ . The IR studies provide data about the structural formation of the spinel ferrite. The observed band positions from IR results as shown in table 3. IR results indicate two prominent bands around  $600$  and  $400\text{ cm}^{-1}$  in all samples due to vibrations of tetrahedral and octahedral sites [18]. Hence, confirm the prepared samples having a single phase with a homogenous structure.

The observed frequency bands ( $\nu_1$ ) in the range of  $557$  to  $577\text{ cm}^{-1}$  are considered as the high-frequency bands (strong absorption), whereas the frequency bands ( $\nu_2$ ) in the range of  $418$  to  $420\text{ cm}^{-1}$  are considered to be the low-frequency bands (weak absorption). The increase in calcination temperature causes an increase in the high-frequency bands and lower frequency bands [19]. The  $Ni^{2+}$  ions substituted at (A) site, shifting the proportional number of  $Fe^{2+}$  ion from A to B site, causes to enhance in the cation-oxygen bond length of tetrahedral lattice site (A) of spinel ferrite

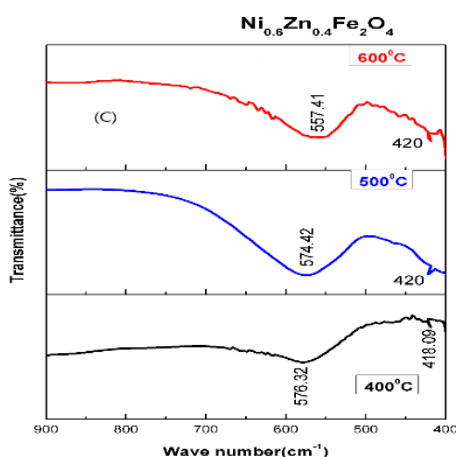


Fig. 6. IR spectra for  $Ni_{0.6}Zn_{0.4}Fe_2O_4$  nano ferrite specimens calcined at  $400^{\circ}C$ ,  $500^{\circ}C$  and  $600^{\circ}C$ .

Table 3. FTIR band positions of  $Ni_{0.6}Zn_{0.4}Fe_2O_4$  at  $400^{\circ}C$ ,  $500^{\circ}C$  and  $600^{\circ}C$  calcination temperatures.

Concentration (X)	Calcination temperature ( $^{\circ}C$ )	Higher Frequency band ( $\nu_1$ ) $cm^{-1}$	Lower Frequency band ( $\nu_2$ ) $cm^{-1}$
$Ni_{0.6}Zn_{0.4}Fe_2O_4$	400	576.32	418.09
	500	574.42	420
	600	557.41	420

### 3.5. Dielectric properties

#### 3.5.1. Dielectric constant

The behaviour of dielectric constant (K) with  $\ln(f)$  in the frequency range 1Hz to 1MHz for  $Ni_{0.6}Zn_{0.4}Fe_2O_4$  calcined at  $400^{\circ}C$ ,  $500^{\circ}C$  and  $600^{\circ}C$  as shown in figure 7. The dielectric constant (K) of Ni-doped Zn ferrite at 300k has been measured by using formula 3. All the samples are sintered at  $800^{\circ}C$ . The values of dielectric constant (K) decrease with increasing the frequency. At a certain frequency, the observed dielectric constant is unchanged and independent on frequency, possess normal behaviour of ferromagnetic material.

$$K = C d / \epsilon_0 A \quad (3)$$

K----- is dielectric constant

d----- thickness of the sample

A----- Area of the sample

C----- capacitance of a capacitor with a dielectric

#### 3.5.2. Effect of frequency on dielectric constant

The dielectric constant (K) described based on the Maxwell–Wagner type of interfacial polarization that has an adequate agreement with Koop's theory [20]. Ferrites comprise of conducting grain with weak grain boundaries. Initially, the electrons follow the applied field and piled up at the grain boundaries through the exchange mechanism that forms polarization. However, at a specific frequency, the hopping of electrons between  $Fe^{2+}/Fe^{3+}$  ions can not follow the field, and it consumes a definite time to align in the field direction that triggers to reduce the polarization. Hence the dielectric constant decreases.

Fig 7. illustrates the changing of dielectric constant with increasing frequency calcined at  $400^{\circ}C$ ,  $500^{\circ}C$  and  $600^{\circ}C$ . The enhancement of dielectric constant with calcination temperature is mainly due to that more  $Ni^{2+}$  ions occupy A sites instead of  $Fe^{3+}$  ions. Hence, the number of  $Fe^{3+}$  ions migrate to B site, causes more concentration of  $Fe^{3+} \leftrightarrow Fe^{2+}$  ion pairs at the B-site and consequently the amount of space charge polarization increases, leads to increase the values of dielectric constant [21].

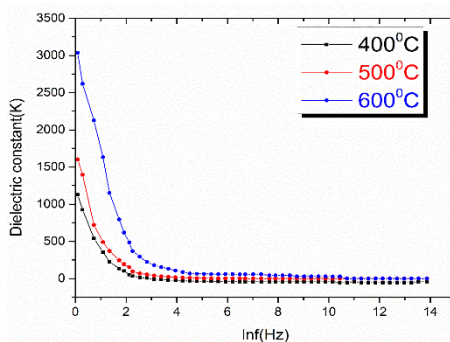


Fig. 7. Variation of the dielectric constant of  $Ni_{0.6}Zn_{0.4}Fe_2O_4$  ferrite nanoparticles calcined at  $400^{\circ}C$ ,  $500^{\circ}C$  and  $600^{\circ}C$ .

### 3.6. Magnetic properties

Fig. 8 indicates the M-H curves of  $Ni_{0.6}Zn_{0.4}Fe_2O_4$  sample analyzed at room temperature using a vibrating sample magnetometer with a maximum field of  $\pm 15$  (kOe) calcinated at  $400^\circ C$ ,  $500^\circ C$  and  $600^\circ C$ . The derived values of saturation magnetization ( $M_s$ ), residual magnetization ( $M_r$ ) and coercivity ( $H_c$ ) are mentioned in table 4. It can be observed that the values of the saturation magnetization  $M_s$  and remanent magnetization  $M_r$  are increased by increasing the temperature from  $400^\circ C$  to  $600^\circ C$ , which arising from spin non-colinearity at the surface of the crystals. The changes in the magnetic properties of the nanoparticles can be attributed to the modification of the crystallinity and crystallite size dependent on the calcination temperature. The variation of coercivity ( $H_c$ ) opposite to that of  $M_s$  and  $M_r$ , indicating that  $H_c$  was not determined only by the size of nanoparticles [22, 23].

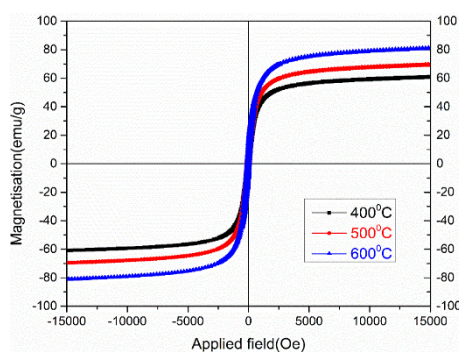


Fig. 8. M-H curve of  $Ni_{0.6}Zn_{0.4}Fe_2O_4$  ferrite nanoparticles calcination at  $400^\circ C$ ,  $500^\circ C$  and  $600^\circ C$ .

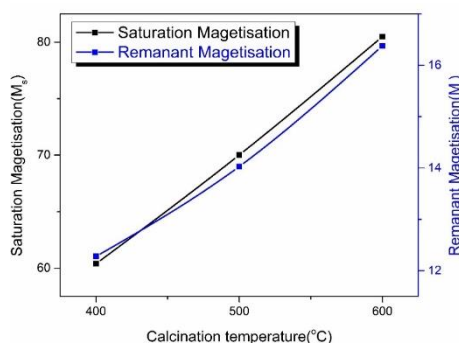


Fig. 9. Variation of  $M_s$  and  $M_r$  values of  $Ni_{0.6}Zn_{0.4}Fe_2O_4$  ferrite nanoparticles calcination at  $400^\circ C$ ,  $500^\circ C$  and  $600^\circ C$ .

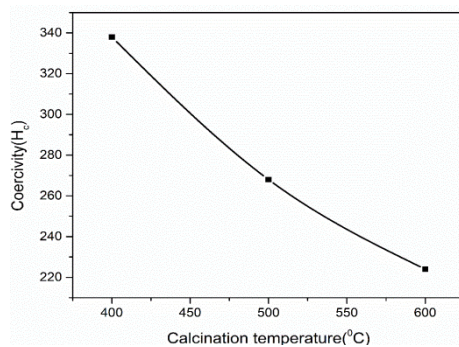


Fig 10. Variation  $H_c$  values of  $Ni_{0.6}Zn_{0.4}Fe_2O_4$  ferrite nanoparticles calcination at  $400^\circ C$ ,  $500^\circ C$  and  $600^\circ C$ .

Table 4. Dependence of  $M_s$ ,  $M_r$  and  $H_c$  values of  $Ni_{0.6}Zn_{0.4}Fe_2O_4$  ferrite nanoparticles at  $400^\circ C$ ,  $500^\circ C$  and  $600^\circ C$ .

Calcination Temperature	Composition	$M_s$ (emu/g)	$M_r$ (emu/g)	$H_c$ (Oe)
$400^\circ C$	$Ni_{0.6}Zn_{0.4}Fe_2O_4$	61.077	12.28	338
$500^\circ C$		70.25	14.03	268
$600^\circ C$		80.7978	16.37	224

#### 4. Conclusions

In summary, effects of calcination temperature on the physical properties and crystallinity of  $Ni_{0.6}Zn_{0.4}Fe_2O_4$  ferrite nanoparticles successfully synthesized by sol-gel auto combustion method have been investigated with the aim of the dependence of physical properties on the crystallite size and expanding the range of applications. Our results showed that the dielectric constant and magnetic properties of the  $Ni_{0.6}Zn_{0.4}Fe_2O_4$  nanoparticles were strongly affected by the calcination temperature as a consequence of the gradual increase in the crystallinity and particle size. Therefore, ideal magnetic properties and behaviour of  $Ni_{0.6}Zn_{0.4}Fe_2O_4$  nanoparticles can be achieved by changing the calcination temperature.

#### Acknowledgements

The author greatly indebted to Authors are thankful to *Dr Panthagani Raju*, Department of Physics, Osmania University, Hyderabad, India, for his support to carry out the LCR measurements.

#### References

- [1] H. Deng, X. L. Li, Q. Peng, X. Wang, J. P. Chen, Y. D. Li, *Angew Chem Int Ed* **44**, 2782 (2005).
- [2] E. Pervaiz, I. H. Gul, H. Anwar, *J Supercond Nov Magn.* **26**, 415 (2013).
- [3] M. Bellusci, S. Canepari, G. Ennas, A. L. Barbera, F. Padella, A. Santini, A. Scano, L. Seralessandri, F. Varsano, *J Am Ceram Soc* **90**, 3977 (2007).
- [4] S. Laurent, D. Forge, M. Port, C. Robic, V. L. Elst, R. N. Muller, *Chem Rev.* **108**, 2064 (2008).
- [5] S. J. Feng, W. Yang, Z. B. Wang, *Mater Sci Eng B.* **176**, 1509 (2011).
- [6] J. Jacob, M. A. Khadar, *J Appl Phys.* **107**, 114 (2010).
- [7] T. Zak, D. Saed, D. Aman, S. A. Younis, Y. M. Moustafa, *J Sol-Gel Sci Technol.* **65**, 269 (2013).
- [8] L. Satyanarayana, K. M. Reddy, V. M. Sunkara, *Mater Chem Phys.* **82**, 21 (2003).
- [9] U. Naresh, R. J. Kumar, K. C. B. Naidu, *Ceram. Int.* **45**, 7515 (2019).
- [10] U. Naresh, R. J. Kumar, K. C. B. Naidu, *Mater. Chem. Phys.* **236**, 121807 (2019).
- [11] T. A. Taha, A. A. Azab, M. A. Sebak, *J. Mol. Struct.* **1181**, 14 (2019).
- [12] P. S. Kumar, K. Thyagarajan, A. G. Kumar, *Digest Journal of Nanomaterials and Biostructures.* **13**(4), 1117 (2018).
- [13] K. C. B. Naidu, W. Madhuri, *Bull. Mater. Sci.* **40**, 417 (2017).
- [14] A. AbuEl-Fadl, A. M. Hassan, M. H. Mahmoud, TetianaTatarchuk, I. P. Yaremiy, A. M. Gismelssed, M. A. Ahmed, *Journal of Magnetism and Magnetic materials* **471**, 192 (2019).
- [15] A. D. Sheikh, A. V. L. Mathe, *J Mater Sci.* **43**, 2018 (2008).
- [16] Preet Pal Singh, I. S. Hudhara, Shashi Bhushan Rana, *Materials Science-Poland* **34**(2), 451 (2016).

- [17] Ashok Kumar, Parmod Kumar, Geeta Rana, M. S. Yadav, R. P. Pant, *Appl. Sci. Lett.* **1**(2), 33 (2015).
- [18] K. Maaz, A. Mumtaz, S. K. Hasanain, Abdullah Ceylan, *Journal of Magnetism and Magnetic Materials* **308**, 289 (2007).
- [19] Sujata Sumant Khot, Neelam Sunil Shinde, Bhimrao Ladgaonkar, B. B. Kale, Shrikant Chintamani Watawe, *International Journal of Advances in Engineering & Technology*, 2231 (2011).
- [20] K. W. Wagner, *Ann. Phys* **40**, 817 (1913).
- [21] Siva Kumar Pendyala, K. Thyagarajan, A. Guru Sampath Kumar, L. Obulapathi, *Journal of microwave power and electromagnetic energy* **3**(1), 3 (2019).
- [22] P. Sivakumar, R. Ramesh, A. Ramanand, S. Ponnusamy, C. Muthamizhchelvan, *Mater Lett* **65**, 483 (2011).
- [23] N. D. S. Mohallem, L. Seara, *Appl Surf Sci* **214**, 143 (2003).